Soft Matter

PAPER

View Article Online
View Journal | View Issue

Cite this: *Soft Matter*, 2014, **10**, 2160

Cholesterol affects C_{60} translocation across lipid bilayers†

Dandan Sun, Xubo Lin and Ning Gu*

Received 17th August 2013
Accepted 13th January 2014

DOI: 10.1039/c3sm52211c

www.rsc.org/softmatter

Cholesterol plays an important role in regulating the structural properties of phospholipid membranes and further influences the permeability of molecules and nanoparticles. However, nanoparticles' translocation across phospholipid membranes in the presence of cholesterol on the molecular scale is rarely studied. Here, we performed coarse-grained molecular dynamics simulations to probe the translocation of C_{60}, one of the most popular nanoparticles, across dipalmitoylphosphatidylcholine bilayers with different concentrations of cholesterol molecules (0–50 mol%). The results reveal that the presence of cholesterol molecules induces lower area per lipid, larger bilayer thickness, and more ordered orientation of lipid tails. The higher the concentration of cholesterol molecules, the more significant is the condensing effect of lipid bilayer as just mentioned. Besides, dynamic processes, free energy profiles and permeability coefficients further indicate that the permeability of C_{60} decreases with increasing cholesterol concentration, which can be explained by the condensation effect and reduced free volume. Our researches provide an explicit description of the impact of cholesterol on C_{60} translocation across lipid bilayers.

Introduction

With the rapid development of nanotechnology, nanoparticles (NPs) are extensively applied in medical and biological studies.[1–3] For example, C_{60}, one of the most popular nanoparticles, has been widely used as X-ray imaging agents,[4] antioxidants against radical-initiated lipid peroxidation,[5] drug carriers,[6] *etc.* In order to obtain better biomedical applications of NPs, much attention should be paid to the effects of NPs on human health and the environment.[7–9] Consequently, it is of great significance to probe the interactions between NPs and cellular components, such as membranes,[10] proteins[11,12] and DNA.[13] In the present work, we focus on the interactions of C_{60} with model cell membranes.

Cell membranes have plentiful components, including various types of lipids, proteins and sterols. In mammalian cellular membranes, cholesterol is the most abundant sterol. Cholesterol produces a striking impact on the structural properties of phospholipid membranes.[14–16] It also plays a non-negligible role in the formation of lipid rafts.[17,18] Additionally, many publications have reported that cholesterol imposes remarkable influences on the permeability of small molecules, such as water,[19] ions,[20] and organic molecules.[21] For instance, Xiang and Anderson[22,23] investigated the permeability of acetic acid in cholesterol-containing lipid bilayers. Saito *et al.*[19] demonstrated a drastic reduction of water permeability with increasing cholesterol concentration in dipalmitoylphosphatidylcholine (DPPC) and palmitoylsphingomyelin (PSM) lipid bilayers. On the contrary, Gensure *et al.*[20] found that the presence of cholesterol could increase proton permeability. However, few systematic researches elucidate the influence of cholesterol on C_{60} translocation through lipid bilayers. Fiedler *et al.*[24] implemented C_{60} permeation through dimyristoylphosphatidylcholine (DMPC) bilayers with 25 mol% cholesterol, yet they were mainly concerned about the influence of nanoparticle morphology (C_{60}, NanoC and open-C_{60}), rather than the influence of cholesterol on C_{60} translocation through lipid bilayers.

There are multiple types of phospholipids, including saturated-chain (DPPC, DMPC *etc.*) and unsaturated-chain (POPC, DAPC *etc.*) phospholipids. The saturation level of the lipid tails greatly influences cholesterol-containing phospholipid bilayers. Marrink *et al.*[25] fulfilled molecular dynamics (MD) simulations for polyunsaturated lipid bilayers with a varying degree of fatty acid unsaturation, revealing drastic differences in orientation and dynamical behavior of cholesterols with increasing saturation level of the lipid tails. Bennett *et al.*[26] also stated that the rate of cholesterol flip-flop depended on the saturation level of the lipids. Our researches primarily focus on the role of cholesterol in C_{60} translocation across cholesterol-containing lipid bilayers. Thus, we chose a simple model, dipalmitoylphosphatidylcholine (DPPC), whose hydrocarbon tails comprise

State Key Laboratory of Bioelectronics, Jiangsu key Laboratory for Biomaterials and Devices, School of Biological Science & Medical Engineering, Southeast University, Nanjing, 210096, People's Republic of China. E-mail: guning@seu.edu.cn; Fax: +86 (0)25-8327-2460

† Electronic supplementary information (ESI) available: The method of diffusion coefficient and permeability coefficient. See DOI: 10.1039/c3sm52211c

only single bonds, to mimic the cell membrane. Lots of studies are available for DPPC bilayers with cholesterols.[15,19,26]

Since the solubility of C_{60} is difficult in the aqueous phase,[10,27] it's a challenge to perform experimental studies of C_{60} permeation through lipid membranes. Computer simulations may be a robust tool to explore the effect of cholesterol on the interactions of C_{60} with lipid bilayers.[28] MD simulations are valuable for studying lipid bilayers[29] and proteins.[30] Several all-atom MD simulations have been executed to address the interactions of pristine C_{60} and its derivatives with lipid bilayers.[31–34] For example, Qiao *et al.*[31] pointed out the two forms of fullerenes affected the structure of membranes differently by studying the translocation of C_{60} and its derivative $C_{60}(OH)_{20}$ across DPPC bilayers. Chang *et al.*[32] presented the structural and dynamic properties of C_{60} clusters in DMPC membranes by constructing four C_{60}–membrane systems, in which C_{60} resided either inside or outside the membranes.

Atomistic simulations can reveal maximum detail but are restricted to small time and length scales. Relatively, coarse-grained (CG) MD simulations have larger time and length scales. There are some aspects of CG models where clusters of several atoms are treated as a single interaction site.[29,35–38] Orsi *et al.*[38] developed a CG approach for DMPC and DOPC, and the models take a complete representation of electrostatics and a realistic description of the water component into consideration. In this work, a simple and popular MARTINI CG model, developed by Marrink,[29] is adopted. Compared with the CG models of Orsi, the MARTINI force field employs a simplified water description and only includes explicit charges in the lipid headgroups. CGMD simulations of C_{60} interactions with lipid bilayers have been generally described in recent years.[39–41] Wong-Ekkabut *et al.*[39] used CGMD simulations to research the interactions of fullerene clusters with lipid bilayers, presenting fullerenes rapidly aggregated in water but disaggregated upon entering the membrane interior. D'Rozario *et al.*[40] performed CGMD simulations to study the interactions of both pristine C_{60} and its various derivatives with DPPC bilayers and revealed the extent of derivatization of C_{60} affected profoundly its interaction with lipid bilayers. Nonetheless, there is no systematic work about the effect of cholesterol on the DPPC bilayers with CGMD simulations.

Hence, we carry out CGMD simulations to gain some insight into the thermodynamics and mechanism of the interactions of C_{60} with DPPC bilayers in the presence of cholesterol. We build 6 different systems containing DPPC, cholesterol and C_{60} molecules. The cholesterol concentrations range from 0 to 50 mol%. For DPPC/cholesterol (DPPC/CHOL) systems, we evaluate the role of cholesterol in the structural properties of DPPC bilayers, including bilayer thickness, area per lipid, and order parameter. Also, the tilt angles of cholesterol molecules are estimated. Afterwards, we derive the potential of mean force (PMF) as a function of position of C_{60} along the bilayer normal, illustrating the large influence of cholesterol on C_{60} translocation across lipid membranes. To characterize the dynamic of C_{60} penetration into the bilayer, the diffusion coefficient and permeability coefficient of C_{60} are also calculated. Remarkably, these results demonstrate that cholesterol affects the structural properties of lipid bilayers and the permeability of C_{60} across lipid bilayers. Moreover, these results may offer profound information about the role of cholesterol in lipid membranes and give some guidelines to the nanomedicine applications of C_{60}.

Simulation methods

We utilize CG models for DPPC/cholesterol/water/C_{60} systems with the MARTINI CG force field developed by Marrink *et al.*[42] In the MARTINI force field, small groups of atoms are represented by a single interaction site. In general, a 4:1 mapping is used to describe the molecules in the simplified model, except in the case of ring structures (benzene, cholesterol *etc.*), where mapping is approximately 2 or 3 to 1. The MARTINI CG models mainly consider four main types of interaction sites: polar (P), nonpolar (N), apolar (C), and charged (Q), each of which has a number of sublevels (0, a, d, ad) or (1, 2, 3, 4, 5). In the present work, the C_{60} model is the same as Wong-Ekkabut's,[39] having similar dimensions with respect to a C_{60} molecule. DPPC and cholesterol models originate from Marrink *et al.*[42] The CG models of DPPC, cholesterol and C_{60} are shown in Fig. 1. For CG water (W), each bead represents four water molecules.

Six systems with various cholesterol concentrations, ranging from 0 to 50 mol%, were initially assembled. Table 1 summarizes the number of molecules in all simulation systems. The DPPC/CHOL molar ratios in each system are 512 DPPC : 0 CHOL (0 mol%), 460 DPPC : 52 CHOL (10 mol%), 410 DPPC : 102 CHOL (20 mol%), 358 DPPC : 154 CHOL (30 mol%), 308 DPPC : 204 CHOL (40 mol%), 256 DPPC : 256 CHOL (50 mol%). Cholesterol molecules were added to the systems by randomly replacing lipid molecules to obtain the desired concentration, and the number of cholesterol molecules remained the same in the two leaflets of the bilayer.

For the sake of concision, we define the mid-plane of the DPPC bilayer as the x–y plane, with the z axis perpendicular to

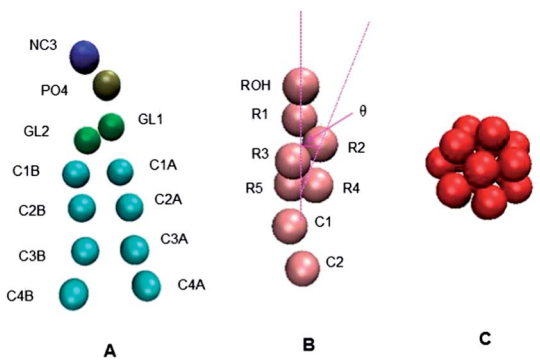

Fig. 1 CG models of DPPC (A), cholesterol (B), and C_{60} (C). A DPPC molecule contains 12 beads, including the headgroup (NC3, PO4), glycerol ester linkage (GL1, GL2) and two tails (C1A–C2A–C3A–C3A, C1B–C2B–C3B–C4B). A cholesterol molecule consists of a hydrophilic head (ROH), a sterol ring body and a hydrophobic tail (C1–C2). The angle between the line connecting the R2 and R4 beads and the bilayer normal is defined as the tilt angle of a cholesterol molecule. A C_{60} molecule has 16 beads.

Table 1 Composition of all simulation systems

System	% cholesterol	# DPPC	# cholesterol	# water
1	0 mol%	512	0	20 000
2	10 mol%	460	52	20 000
3	20 mol%	410	102	20 000
4	30 mol%	358	154	20 000
5	40 mol%	308	204	20 000
6	50 mol%	256	256	20 000

the bilayer. Along the z axis, the lipid leaflet with the larger z values is the upper lipid leaflet and the other is the lower lipid leaflet.

The six systems were energy-minimized by a steepest-descent algorithm. After that, an equilibration of 200 ns was executed with a time step of 20 fs. The dynamic simulation productions were used to evaluate the effect of cholesterol on the structural properties of DPPC bilayers. The final equilibrium configurations were the starting state for the next simulations in which C_{60} interacted with the DPPC/CHOL bilayer. Then we inserted C_{60} into these systems separately to get six new systems, each with a single C_{60}. The C_{60} was initially placed $\sim$1 nm from the upper lipid leaflet. After energy minimization, a pre-equilibration run of 10 ns in each system was processed to remove steric conflicts and obtain stable configurations. Six 300 ns separate MD simulations were carried out with the obtained configurations.

In order to investigate the impact of cholesterol on the structures of DPPC bilayers, some important structural parameters were derived as a function of cholesterol concentration, including area per lipid, bilayer thickness, order parameter, and tilt angles of cholesterol molecules. To study the permeation behavior of C_{60} translocation into DPPC/CHOL bilayers, the PMF (free energy) as a function of position of C_{60} along a reaction coordinate with umbrella sampling[43] was implemented. To characterize the dynamic of C_{60} penetration into the bilayer, we also clarified the diffusion coefficient and permeability coefficient of C_{60}. The reaction coordinate was chosen as the z-directional distance between the center-of-mass (COM) of C_{60} and the center of the DPPC/CHOL bilayer. A series of simulations were performed in which the C_{60} was restrained at some given distances from the center of the bilayer using a harmonic potential, utilizing a force constant of 1000 kJ mol^{-1} nm^{-2} for the biasing potential in the z direction, while no restraints were applied in the x–y plane. More details about the method can be found elsewhere.[39,40]

We chose 51 independent windows along the reaction coordinate spaced 0.1 nm apart (z = 0 to 5.0 nm; the bilayer center was at 0 nm) for each system. Considering the symmetry of the bilayer, we only processed the upper lipid leaflet. For each window, a 20 ns CGMD simulation was employed, resulting in 61.2 μs of biased simulation in total. Prior to the MD simulations, an equilibration simulation of 1 ns was accomplished to allow the system to reach equilibrium. The PMF profiles were computed with the weighted histogram analysis method (WHAM),[44] as implemented in the g_wham software.[45]

All simulations were carried out by the GROMACS 4.5.4.[46] Simulation parameters were the standard ones with the MARTINI force field. Non-bonded interactions were calculated: a 1.2 nm cutoff with shift function was applied for electrostatic and Lennard-Jones interactions; the distance to start shifting Coulomb and van der Waals interactions was 0 and 0.9 nm, respectively. Under the NPT ensemble and periodic boundary conditions, Berendsen coupling schemes for both pressure (semiisotropic; 1 bar; 0.2 ps coupling time) and temperature (323 K; 1.0 ps coupling time) were used. The timestep of integration was 20 fs. Simulations were visualized using Visual Molecular Dynamics (VMD).[47]

Results and discussion

The effect of cholesterol on the structure of DPPC bilayers

It is well documented that cholesterol has a condensing effect on lipid membranes, arousing an increasing order of the lipid hydrocarbon chains, an increasing of the bilayer thickness and a reduction of the area per lipid with increasing cholesterol concentration.[15,16] In the following we present some important parameters as a function of cholesterol concentration to prove the notable role of cholesterol in regulating the properties of lipid membranes, covering area per lipid, bilayer thickness, order parameter, and tilt angles of cholesterol molecules.

For the 0%-system without cholesterol molecules the area per lipid can be simply obtained through dividing the area of the simulation box by half the number of lipids in the system. The area per lipid of the 0%-system we estimated is 0.631 nm^2. For cholesterol-containing systems, many different methods can be used to determine the area per lipid.[15,48–50] Edholm and Nagle[50] compared three distinct methods, and proposed an improvement of the volumetric part of Hofsäβ *et al.*[15] Considering the complexity of the method of Edholm and the availability of the method of Hofsäβ, the method of Hofsäβ is adopted. The volume of cholesterol is considered to be a constant, independent of cholesterol concentration. Here the area per DPPC can be determined from

$$A_{\mathrm{DPPC}} = \frac{2A}{N_{\mathrm{DPPC}}}\left(1 - \frac{N_{\mathrm{CHOL}} V_{\mathrm{CHOL}}}{V - N_{\mathrm{W}} V_{\mathrm{W}}}\right) \quad (1)$$

where A is the area of the box in the x–y plane, N_{DPPC}, N_{CHOL} and N_{W} are the total number of lipids, cholesterol and water molecules in the system, respectively, and V, V_{CHOL} and V_{W} are the volume of the system, a cholesterol molecule and a water molecule, respectively. The volume of a water molecule can be estimated from a CG water simulation and it is 0.12 nm^3 at 323 K. Since there is an experimental volume of 0.030 nm^3 for a water molecule[51] and a CG water model representing 4 H_2O molecules, the obtained volume is reasonable. The volume of a cholesterol molecule is evaluated from a CG simulation of a small system consisting of 256 cholesterol molecules and 20 000 water molecules at 323 K, by these means a volume of 0.605 nm^3 is obtained. In the previous work, the volume of a cholesterol molecule is 0.619 nm^3,[52] and in view of the different conditions and force fields the difference is acceptable. Nevertheless, Greenwood *et al.*[53] utilized the neutral flotation method

and exhibited that the molecular volume V_L of the lipid and V_C of the cholesterol varied as the mole fractions of cholesterol varied. Here we treat the volume of cholesterol as a constant to make the process simple. The reason why the cholesterol volume (0.605 nm^3) is lower than Greenwood *et al.*'s "bare volume" of 0.630 nm^3 may be the use of the MARTINI CG force field. The values of area per lipid as a function of cholesterol concentration are visualized in Fig. 2. Compared with many simulation data,[15,42] the values of area per lipid we showed are reliable. The area per lipid rapidly decreases in the range of 0–30 mol% of cholesterol, and slowly decreases in the range of 30–50 mol%. This result is in accord with Hofsäβ's.[15] The decreasing trends are also deduced by Pan *et al.* in a DMPC/CHOL bilayer.[54] For the pure DPPC bilayer (0%-system), the area per lipid we calculated is 0.631 nm^2, which is in line with the experimental value of 63.0 $Å^2$.[55] Mills *et al.*[56] demonstrated that the experimental data of 10% and 40% systems were 57.9 $Å^2$ and 52.9 $Å^2$, respectively. The values of 0.602 nm^2 and 0.550 nm^2 in our work are consistent with Mills *et al.*'s. This result convincingly illustrates the condensing effect (the details are given below).

The bilayer thickness is defined as the distance between the upper and lower lipid leaflet, which represents the average distance between the phosphates (PO4) along the bilayer normal. The bilayer thicknesses of the systems are given in Fig. 2. For the 0%-system, the bilayer thickness is 0.405 nm, which satisfies the experimental values of 38.3 Å.[51] Similar variation trends where the bilayer thickness increases rapidly as cholesterol mole fraction c increases to 0.2 and levels off at higher c are also illuminated by Pan *et al.* in a DMPC/CHOL bilayer.[54] The increase in bilayer thickness is probably due to the migration of DPPC headgroups toward the bilayer–aqueous interface to accommodate more cholesterol molecules. Naturally, since the bilayers have incompressible fluidity, the decrease of area per lipid results in a corresponding increasing of bilayer thickness.

As a measure of the orientational order of the lipid tails, we estimate the order parameter,[29] which can be derived from

$$S_z = (3\langle \cos^2 \theta_z \rangle - 1)/2 \quad (2)$$

where θ_z is the angle between the bilayer normal and the molecular axis under consideration. The latter is defined as the vector from C_{n-1} to C_{n-2}. Here the C2A site can be used as a reference point. Perfect alignment with the bilayer normal is indicated by $S_z = 1$, and anti-alignment by $S_z = -0.5$. We calculate order parameters for these systems averaging over 150–200 ns. The order parameters are displayed in Fig. 3. Both the experimental data and the simulations illustrate that cholesterol increases the order of lipid tail chains, which is agreement with previous work.[15,16,19] However, the variations in the results we calculated are discrepant with the experimental data by Pan *et al.*[54] and Mills *et al.*[56] Mills *et al.*'s profile increased monotonically as a function of cholesterol

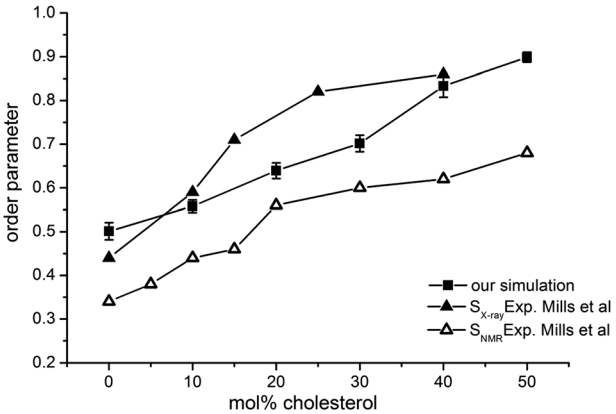

Fig. 3 Order parameters of DPPC molecules as a function of cholesterol concentration. We compare the results of our simulation with the experimental data of Mills *et al.*[56]

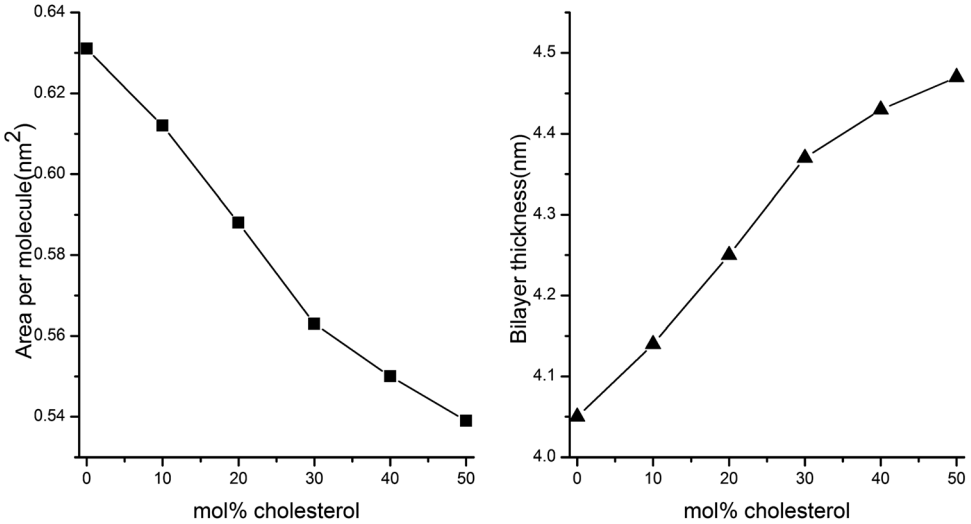

Fig. 2 Area per molecule (left) and bilayer thickness (right) of the six DPPC/CHOL systems as a function of cholesterol concentration.

concentration and began to level off at ~25 mol%. Pan *et al.* characterized the data in terms of a leveling off at ~20 mol%. Our data increase slowly at higher concentration but don't have an obvious flat region. Meyer *et al.*[16] concluded a similar trend in DMPC/cholesterol systems with CGMD simulations. The reason may lie in CG models. For the MARTINI force field a CG site corresponds to the center-of-mass of four adjacent methylene groups in the atomistic model. The CG models neglect the information about atomistic bonds and this is the imperfection of CG simulations. This viewpoint has also been proposed by Marrink *et al.*,[29] and they inferred that the order parameters of CG models couldn't be directly compared to experimental bond order parameters.

The tilt angle of a cholesterol molecule is determined as the angle between the line connecting the R2 and R4 beads and the bilayer normal (*z* axis) (Fig. 1). The distributions of tilt angles are plotted in Fig. 4. As the number of the cholesterol molecules increases, the tilt angles are shifted to smaller angles and the distributions become sharper, suggesting that the cholesterol molecules are more orientationally ordered and aligning themselves more parallel to the bilayer normal. In other words, the shift to lower values again demonstrates that cholesterols induce the increasing order of lipid chains. The tilt angle of cholesterol, 17°, in the 20%-system, meets the experimental value of 16–19°,[57] as well as agreeing with previous simulations.[58,59] Compared with another study,[60] though the average tilts have differences, the variation tendency is analogous. In addition, there is an inverse correlation between the tilt angles of cholesterols and the ordering ability of lipids, and the increasing ordering of lipids also anticipates a lower tilt angle of the cholesterol.

In summary, cholesterol modifies the properties of lipid bilayers by reducing the area per lipid, increasing the bilayer thickness and increasing the ordering of the phospholipid acyl chains. The reason may be interpreted by the condensing effect.[16,61] The condensing effect can be simply described in terms of the average area per molecule: the area per molecule of a cholesterol-containing lipid bilayer is less than that of the pure lipid bilayer. Different conceptual models have been suggested to explain the condensing effect, including the condensed-complexes model,[62] the superlattice model,[63] and the umbrella model.[64] In our research, the umbrella model may be an elegant statement to expound the interactions of DPPC with cholesterols. The umbrella model proposes that the headgroup (ROH) of cholesterol is too small to cover its larger hydrophobic ring body, and therefore the polar phospholipid headgroups of DPPC need to contribute to the screening of the cholesterol molecules from water. Cholesterol molecules squeeze into the DPPC acyl chain region to avoid exposure to water and partially hide themselves under the headgroups of neighboring PCs, forming "umbrellas". The acyl tails need to be straightened to make space for cholesterols, resulting in the increase of order parameters. The headgroups of DPPC expand toward the bilayer–aqueous interface to cover more cholesterol molecules, arising in an increase of bilayer thickness and the reduction of area per lipid. The condensing effect and the rigidity of the cholesterol ring structure impose a positive influence on the decrease of the tilt angles of cholesterol molecules. The higher the cholesterol mole fraction (here for 0–50 mol%), the larger the condensing effect.

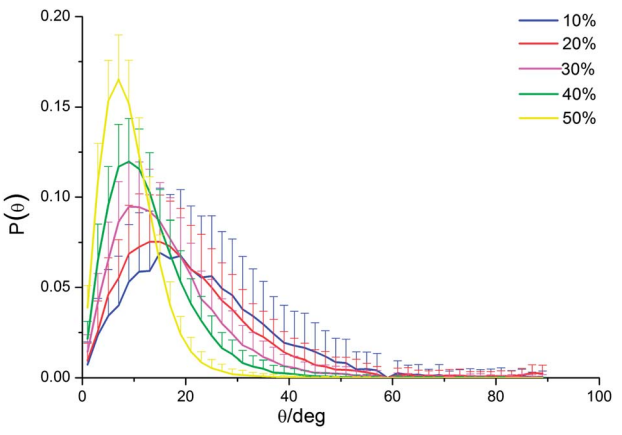

Fig. 4 Tilt angles of cholesterol molecules in DPPC/CHOL bilayers at cholesterol concentrations of 10 mol% (blue), 20 mol% (red), 30 mol% (magenta), 40 mol% (green), and 50 mol% (yellow).

The effect of cholesterol on C_{60} translocation across DPPC bilayers

After six individual 300 ns MD simulations, we analyze simulation trajectories to characterize the dynamics of C_{60}. Fig. 5 depicts the COM positions of C_{60} at various cholesterol mole fractions. Inset (A) shows the histogram of the *z*-coordinate of the COM of C_{60} after C_{60} enters the bilayer; inset (B) shows the side view of the stable simulation system. We observed that the C_{60} was initially placed ~1 nm from the upper lipid leaflet, that is, in bulk water, spontaneously entered the bilayer. All C_{60} molecules rapidly passed into and became entrapped in the bilayer tails region. The transport of C_{60} into the lipid bilayer is driven by the hydrophobic interactions between the C_{60} and the lipid tails. Furthermore, we didn't observe C_{60} translocation outside during the 300 ns MD simulation, resulting from the large energy barrier transferring from the bilayer to bulk water. Inside the bilayer, the equilibrium *z* coordinates of C_{60} are also different in 0–50% systems, corresponding to ~0.98 nm, ~1.13 nm, ~1.16 nm, ~1.24 nm, ~1.45 nm, ~1.58 nm, respectively. Besides, our DPPC/CHOL bilayers didn't disrupt, except the local fluctuations surrounding C_{60}, consistent with Lin *et al.*[65] We also observed that DPPC/CHOL bilayers became tighter and thicker, confirming the effect of cholesterol on the DPPC bilayers mentioned above. The previous reports have similar observations in both atomistic[31,32] and CG[28,39,40] simulations. The preference of C_{60} to be ~1 nm away from the center of the bilayer in the pure bilayer has also been expounded by Wong-Ekkabut.[39] In our MD simulations, the stable *z* coordinates of C_{60} increase as the cholesterol concentration increases. The results are consistent with PMF profiles (the detail is shown above).

To clarify the permeation behavior of C_{60} into DPPC/CHOL bilayers at various cholesterol concentrations, we employ a

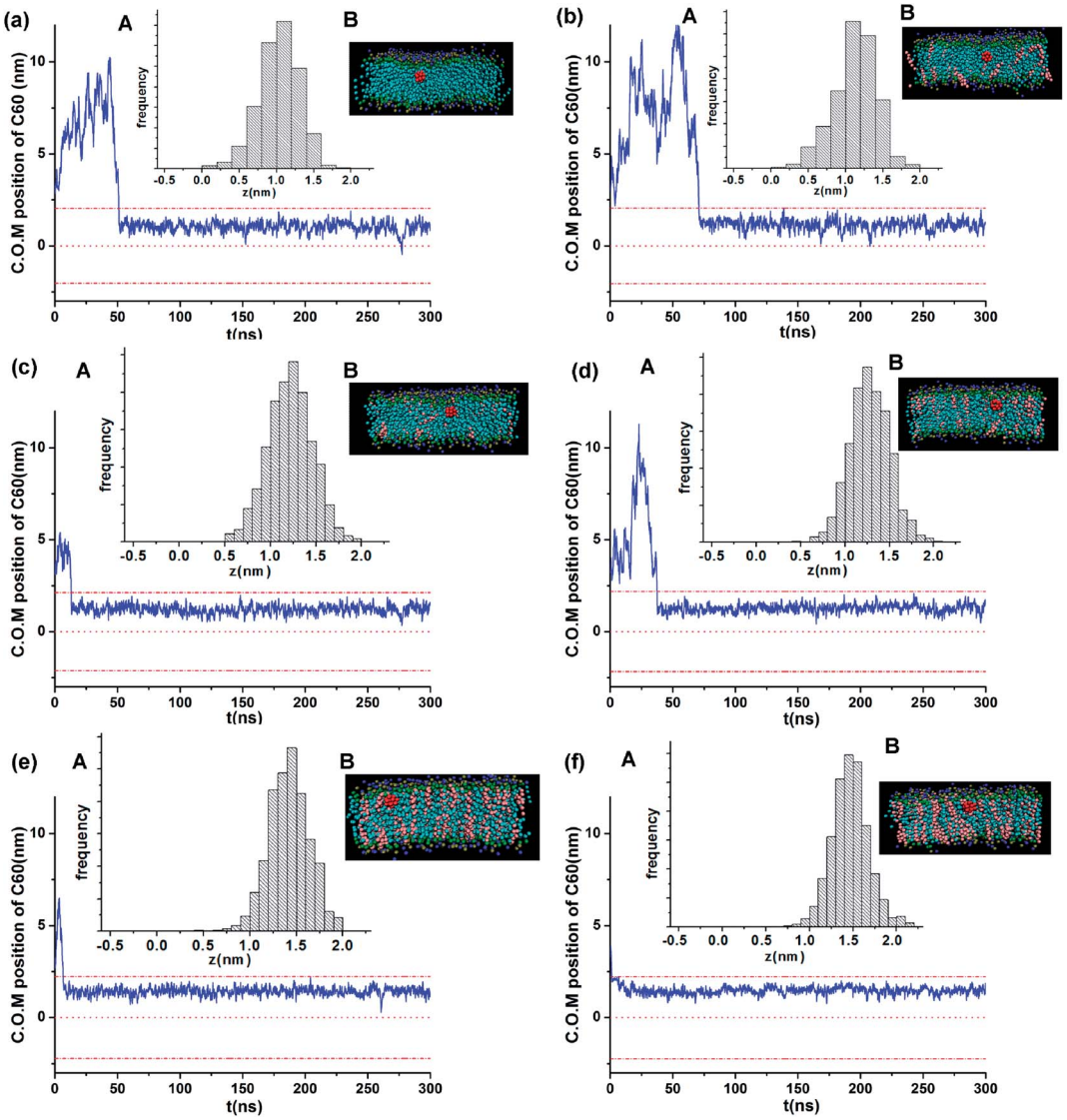

Fig. 5 Trajectories of C_{60} molecules along the z axis during the unbiased MD simulations of six DPPC/CHOL systems at cholesterol concentrations of (a) 0 mol%, (b) 10 mol%, (c) 20 mol%, (d) 30 mol%, (e) 40 mol%, and (f) 50 mol%. The two short dash dotted lines (red) depict the phosphate particles' peak density of the upper and lower leaflet of DPPC bilayers. The dotted lines (red) represent the center of the DPPC/CHOL bilayers. The blue solid lines indicate the COM positions of C_{60}. Inset (A) shows the histogram of the z-coordinate of the COM of C_{60} after C_{60} enters the bilayer; inset (B) shows the side view of the stable simulation system. The C_{60} molecules are shown as red beads, the lipid tail groups as cyan beads, GLY as green beads, the lipid head groups as the tan and blue beads, cholesterol molecules as pink beads. The water molecules as well as DPPC molecules before C_{60} are omitted for clarity. The snapshots were rendered using VMD.

series of PMF profiles to estimate the free energy as a function of the position of the C_{60} molecule along the bilayer normal from the aqueous phase to the center of the bilayer (Fig. 6). All the lines have a similar tendency. Although there are small energy barriers, C_{60} can spontaneously transport into the bilayer in all systems. For the 0%-system, the PMF shows consistency with previous atomistic[31,33] and CG[28,39,40] simulations, though there are differences in the depth of the minimum energy in the bilayer tail region (-72.15 kJ mol^{-1} in our work *versus* -80 kJ mol^{-1} in Monticelli,[28] -110 kJ mol^{-1} in Wong-Ekkabut *et al.*,[39] -74 k_BT in D'Rozario *et al.*[40]). The average positions of the COM of C_{60} yielded in the equilibrium simulations (see above), are quantitatively consistent with the energy wells in the PMF profiles. Namely, our PMF results accord with the unrestrained simulations where C_{60} molecules dwell in the DPPC bilayer tail region. Moreover, as the cholesterol concentration increases, the positions of the energy wells are shifted farther from the bilayer center, corresponding to an increase in the bilayer thickness.

To characterize the dynamic of C_{60} penetration into the bilayer, we calculate the diffusion coefficient and permeability coefficient of C_{60} (see ESI†). The diffusion coefficients $D(z)$ of C_{60} are represented in Fig. S1.† Within the bilayer the diffusion coefficients of C_{60} are significantly smaller than those in bulk water. The diffusion coefficients increase near the center of the bilayer on account of a larger free volume. We observe reductive

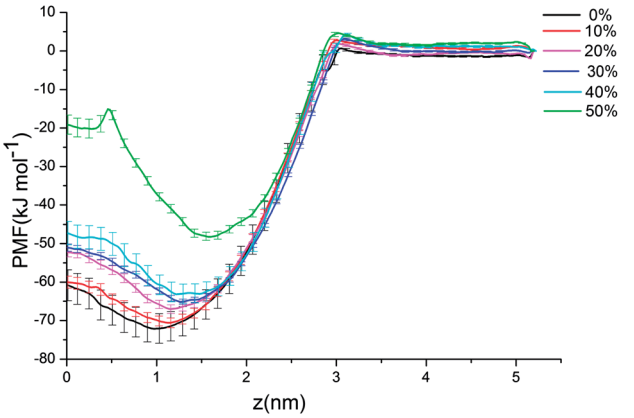

Fig. 6 PMF profiles as a function of the position of the C_{60} molecule along the bilayer normal. The colors of the curves represent the DPPC/CHOL bilayers at cholesterol concentrations of 0 mol% (black), 10 mol% (red), 20 mol% (magenta), 30 mol% (blue), 40 mol% (cyan), and 50 mol% (green). A distance of zero corresponds to the center of the bilayer.

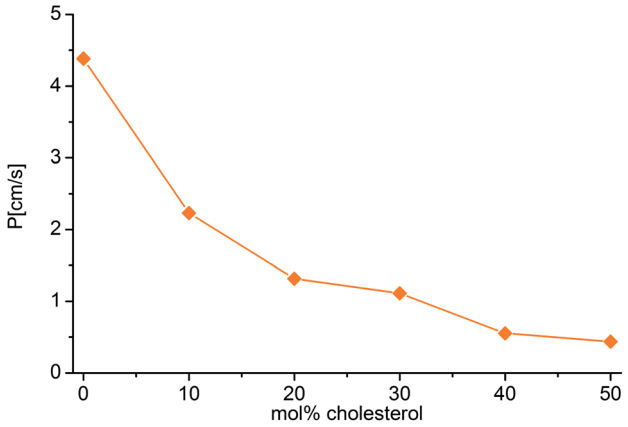

Fig. 7 C_{60} permeability coefficients of DPPC/CHOL bilayers as a function of cholesterol concentration.

diffusion coefficients in relatively dense systems of 40% and 50%, however, we couldn't find an obvious impact of cholesterol on the diffusion coefficients of C_{60} in six systems. Since the cholesterol-containing bilayers are not homogeneous environments, we have to note that the calculated diffusion coefficients are estimated. Adequate initial coordinates in the x–y plane at each z should be sampled in subsequent simulations. For the bilayer without cholesterol molecules, our results are in agreement with other researches. Wong-Ekkabut *et al.*[39] declared fullerene diffused more slowly in the bilayer than in the water layer. Bedrov *et al.*[33] stated that the diffusion coefficients of fullerenes had relatively little dependence on the positions of fullerenes inside the membranes.

The permeability coefficient P can be assessed as[66,67]

$$\frac{1}{P} = \int_0^{5.0} \frac{\exp(\Delta G(z)/RT)}{D(z)} \mathrm{d}z \quad (3)$$

where R is the universal gas constant, T is the absolute temperature, $\Delta G(z)$ is the free energy of solute transferring from water into the membrane, and $D(z)$ is the diffusion coefficient. Fig. 7 plots the permeability coefficients of C_{60} as a function of cholesterol concentration. For the 0%-system, the permeability coefficient we estimated is 4.38 cm s^{-1}, higher than for water[68] and lower than for benzene.[68] Wong-Ekkabut *et al.*[39] measured fullerene permeability in a DOPC bilayer at 300 K and the permeability coefficient was 6×10^{-2} cm s^{-1}. Given the temperature dependence of the permeation process,[66,67] it is reasonable that our results are larger than Wong-Ekkabut's. Marrink and Berendsen[66,67] have also discussed the temperature conversion in researching the permeation of water and assumed an Arrhenius type of temperature dependence. Besides, we should notice that the calculated permeability coefficients depend largely on the position of the integration boundaries.[67] For example, integrating well into $z = 3.3$ nm, Fiedler *et al.*[24] calculated the permeability coefficient of C_{60} as 330 cm s^{-1}. We find that the estimated C_{60} permeability coefficients decrease with increasing cholesterol concentration. The effect of cholesterol on the permeability coefficients of small molecules has been reported. Saito *et al.*[19] investigated the role of cholesterol in water permeability through DPPC/cholesterol bilayers and measured that the water permeability was reduced from 2.6×10^{-1} cm s^{-1} (0 mol%) to 3.7×10^{-4} cm s^{-1} (50 mol%). Wennberg *et al.*[21] derived six different solutes permeating four types of phospholipids membranes and suggested that cholesterol reduced the solutes' permeability much more strongly than expected from permeation experiments on macroscopic membranes.

The reduction in C_{60} permeability through different mole fractions of DPPC/CHOL bilayers can be attributed to the structural characteristics in the presence of cholesterol molecules. A supported explanation is the reduced free volume in the bilayers with increasing cholesterol concentration,[19,21,69] as well as the condensing effect. In the DPPC membranes without cholesterols, the free volume is abundant and the molecular interactions are relatively weak. In consequence, C_{60} transporting into the DPPC bilayer is quite easy and only a few molecular interactions are required to be broken. Nonetheless, in the presence of cholesterol, the lipid tails are more ordered and the membranes' compressibility decreases, in which the bilayers are tightly packed. These induce favorable van der Waals interactions to form in the lipid tail regions. When the C_{60} transports into the lipid bilayer, it is required to break larger molecular interactions, leading to the reduction of C_{60} permeability. The larger the cholesterol concentration, the stronger the intermolecular interactions that need to be destroyed. Similar results have already been published by other researchers. Saito *et al.*[19] explained that the reduced cavity density around the cholesterol was the main reason for reducing the water permeability with increasing cholesterol concentration. Wennberg *et al.*[21] argued that the cost of breaking van der Waals interactions between the lipid tails of cholesterol-containing membranes accounted for the reduced partitioning. It is reasonable to speculate that C_{60} permeability in DPPC/CHOL bilayers becomes smaller and smaller with increasing cholesterol concentration.

Conclusions

The impact of cholesterol on C_{60} translocation across DPPC/CHOL bilayers at various cholesterol concentrations (0–50 mol%) is investigated. We employ a series of CGMD simulations to confirm the condensation effect of cholesterols on DPPC bilayers. The area per lipid rapidly decreases in 0–30 mol% of cholesterol and it's in agreement with experimental results. The presence of cholesterol also makes the bilayer thicken and leads to an increase in the order parameter of the lipid tails. Besides, the tilt angle distributions of cholesterol molecules are shifted to smaller angles, indicating that the cholesterol molecules are aligning themselves more parallel to the bilayer normal. The umbrella model may be responsible for the condensation effect.

Subsequently, we obtain all the dynamics trajectories of the C_{60} molecules in six various DPPC/CHOL bilayers. The C_{60} molecules spontaneously enter the bilayers and entrap in the bilayer tails region with different equilibrium z coordinates. There are only local fluctuations surrounding the C_{60} molecules and no membrane disruption. Computationally, the PMF profiles show slight energy barriers and have shallower energy wells with increasing cholesterol concentration. The diffusion coefficients and permeability coefficients of C_{60} molecules have also been calculated. The estimated C_{60} permeability coefficients decrease with increasing cholesterol concentration. The reasons are the condensation effect and the reduced free volume with the addition of cholesterol. Our results may contribute to comprehending the role of cholesterol molecules in cell membranes and make better use of C_{60} fullerenes in biomedical fields.

Conflict of interest

The authors declare no competing financial interest.

Acknowledgements

The authors thank Qiongying Jia, Zhenzhen Zhang for their careful reading of the manuscript and insightful suggestions in writing. We acknowledge the support of this research from the National Important Basic Research Program of China (no. 2011CB933503), the National Natural Science Foundation of China (no. 61127002), the Basic Research Program of Jiangsu Province (no. BK2011036), and the Outstanding Ph.D. Student Program of China's Ministry of Education.

References

1 C. E. Ashley, E. C. Carnes, G. K. Phillips, D. Padilla, P. N. Durfee, P. A. Brown, T. N. Hanna, J. W. Liu, B. Phillips, M. B. Carter, N. J. Carroll, X. M. Jiang, D. R. Dunphy, C. L. Willman, D. N. Petsev, D. G. Evans, A. N. Parikh, B. Chackerian, W. Wharton, D. S. Peabody and C. J. Brinker, *Nat. Mater.*, 2011, **10**, 389–397.
2 X. Liu, Z. Zhong, Y. Tang and B. Liang, *J. Nanomater.*, 2013, 902538.
3 A. Chen and S. Chatterjee, *Chem. Soc. Rev.*, 2013, **42**, 5425–5438.
4 T. Wharton and L. J. Wilson, *Bioorg. Med. Chem.*, 2002, **10**, 3545–3554.
5 I. C. Wang, L. A. Tai, D. D. Lee, P. P. Kanakamma, C. K. F. Shen, T. Y. Luh, C. H. Cheng and K. C. Hwang, *J. Med. Chem.*, 1999, **42**, 4614–4620.
6 N. Venkatesan, J. Yoshimitsu, Y. Ito, N. Shibata and K. Takada, *Biomaterials*, 2005, **26**, 7154–7163.
7 W. H. Suh, K. S. Suslick, G. D. Stucky and Y. H. Suh, *Prog. Neurobiol.*, 2009, **87**, 133–170.
8 K. Luyts, D. Napierska, B. Nemery and P. H. M. Hoet, *Environ. Sci.: Processes Impacts*, 2013, **15**, 23–38.
9 C. Levard, E. M. Hotze, G. V. Lowry and G. E. Brown, *Environ. Sci. Technol.*, 2012, **46**, 6900–6914.
10 G. Rossi, J. Barnoud and L. Monticelli, *Phys. Scr.*, 2013, **87**, 058503.
11 H. Benyamini, A. Shulman-Peleg, H. J. Wolfson, B. Belgorodsky, L. Fadeev and M. Gozin, *Bioconjugate Chem.*, 2006, **17**, 378–386.
12 E. G. Makarova, R. Y. Gordon and I. Y. Podolski, *J. Nanosci. Nanotechnol.*, 2012, **12**, 119–126.
13 H. An and B. Jin, *Environ. Sci. Technol.*, 2011, **45**, 6608–6616.
14 T. Róg, M. Pasenkiewicz-Gierula, I. Vattulainen and M. Karttunen, *Biochim. Biophys. Acta*, 2009, **1788**, 97–121.
15 C. Hofsäß, E. Lindahl and O. Edholm, *Biophys. J.*, 2003, **84**, 2192–2206.
16 F. de Meyer and B. Smit, *Proc. Natl. Acad. Sci. U. S. A.*, 2009, **106**, 3654–3658.
17 H. J. Risselada and S. J. Marrink, *Proc. Natl. Acad. Sci. U. S. A.*, 2008, **105**, 17367–17372.
18 D. Hakobyan and A. Heuer, *J. Phys. Chem. B*, 2013, **117**, 3841–3851.
19 H. Saito and W. Shinoda, *J. Phys. Chem. B*, 2011, **115**, 15241–15250.
20 R. H. Gensure, M. L. Zeidel and W. G. Hill, *Biochem. J.*, 2006, **398**, 485–495.
21 C. L. Wennberg, D. van der Spoel and J. S. Hub, *J. Am. Chem. Soc.*, 2012, **134**, 5351–5361.
22 T.-X. Xiang and B. D. Anderson, *J. Membr. Biol.*, 1995, **148**, 157–167.
23 T.-X. Xiang and B. D. Anderson, *Biophys. J.*, 1997, **72**, 223–237.
24 S. L. Fiedler and A. Violi, *Biophys. J.*, 2010, **99**, 144–152.
25 S. J. Marrink, A. H. de Vries, T. A. Harroun, J. Katsaras and S. R. Wassall, *J. Am. Chem. Soc.*, 2008, **130**, 10–11.
26 W. F. D. Bennett, J. L. MacCallum, M. J. Hinner, S. J. Marrink and D. P. Tieleman, *J. Am. Chem. Soc.*, 2009, **131**, 12714–12720.
27 R. S. Ruoff, D. S. Tse, R. Malhotra and D. C. Lorents, *J. Phys. Chem.*, 1993, **97**, 3379–3383.
28 L. Monticelli, *J. Chem. Theory Comput.*, 2012, **8**, 1370–1378.
29 S. J. Marrink, A. H. de Vries and A. E. Mark, *J. Phys. Chem. B*, 2004, **108**, 750–760.
30 S. A. Shaikh, J. Li, G. Enkavi, P. C. Wen, Z. Huang and E. Tajkhorshid, *Biochemistry*, 2013, **52**, 569–587.

31 R. Qiao, A. P. Roberts, A. S. Mount, S. J. Klaine and P. C. Ke, *Nano Lett.*, 2007, **7**, 614–619.
32 R. Chang and J. Lee, *Bull. Korean Chem. Soc.*, 2010, **31**, 3195–3200.
33 D. Bedrov, G. D. Smith, H. Davande and L. Li, *J. Phys. Chem. B*, 2008, **112**, 2078–2084.
34 L. Li, H. Davande, D. Bedrov and G. D. Smith, *J. Phys. Chem. B*, 2007, **111**, 4067–4072.
35 J. C. Shelley, M. Y. Shelley, R. C. Reeder, S. Bandyopadhyay and M. L. Klein, *J. Phys. Chem. B*, 2001, **105**, 4464–4470.
36 M. Kranenburg, J. P. Nicolas and B. Smit, *Phys. Chem. Chem. Phys.*, 2004, **6**, 4142–4151.
37 S. Izvekov and G. A. Voth, *J. Phys. Chem. B*, 2005, **109**, 2469–2473.
38 M. Orsi, J. Michel and J. W. Essex, *J. Phys.: Condens. Matter*, 2010, **22**, 155106.
39 J. Wong-Ekkabut, S. Baoukina, W. Triampo, I. M. Tang, D. P. Tieleman and L. Monticelli, *Nat. Nanotechnol.*, 2008, **3**, 363–368.
40 R. S. G. D'Rozario, C. L. Wee, E. J. Wallace and M. S. P. Sansom, *Nanotechnology*, 2009, **20**, 115102.
41 K. Lai, B. Wang, Y. Zhang and Y. Zheng, *Phys. Chem. Chem. Phys.*, 2013, **15**, 270–278.
42 S. J. Marrink, H. J. Risselada, S. Yefimov, D. P. Tieleman and A. H. de Vries, *J. Phys. Chem. B*, 2007, **111**, 7812–7824.
43 J. Kästner, *Wiley Interdiscip. Rev.: Comput. Mol. Sci.*, 2011, **1**, 932–942.
44 S. Kumar, D. Bouzida, R. H. Swendsen, P. A. Kollman and J. M. Rosenberg, *J. Comput. Chem.*, 1992, **13**, 1011–1021.
45 J. S. Hub, B. L. de Groot and D. van der Spoel, *J. Chem. Theory Comput.*, 2010, **6**, 3713–3720.
46 B. Hess, C. Kutzner, D. van der Spoel and E. Lindahl, *J. Chem. Theory Comput.*, 2008, **4**, 435–447.
47 W. Humphrey, A. Dalke and K. Schulten, *J. Mol. Graphics*, 1996, **14**, 33–38.
48 S. W. Chiu, E. Jakobsson, R. J. Mashl and H. L. Scott, *Biophys. J.*, 2002, **83**, 1842–1853.
49 M. H. Cheng, L. T. Liu, A. C. Saladino, Y. Xu and P. Tang, *J. Phys. Chem. B*, 2007, **111**, 14186–14192.
50 O. Edholm and J. F. Nagle, *Biophys. J.*, 2005, **89**, 1827–1832.
51 J. F. Nagle and S. Tristram-Nagle, *Biochim. Biophys. Acta*, 2000, **1469**, 159–195.
52 Z. Cournia, G. M. Ullmann and J. C. Smith, *J. Phys. Chem. B*, 2007, **111**, 1786–1801.
53 A. I. Greenwood, S. Tristram-Nagle and J. F. Nagle, *Chem. Phys. Lipids*, 2006, **143**, 1–10.
54 J. Pan, S. Tristram-Nagle and J. F. Nagle, *Phys. Rev. E: Stat., Nonlinear, Soft Matter Phys.*, 2009, **80**, 021931.
55 N. Kučerka, J. F. Nagle, J. N. Sachs, S. E. Feller, J. Pencer, A. Jackson and J. Katsaras, *Biophys. J.*, 2008, **95**, 2356–2367.
56 T. T. Mills, G. E. S. Toombes, S. Tristram-Nagle, D. M. Smilgies, G. W. Feigenson and J. F. Nagley, *Biophys. J.*, 2008, **95**, 669–681.
57 R. Murari, M. P. Murari and W. J. Baumann, *Biochemistry*, 1986, **25**, 1062–1067.
58 S. Pöyry, T. Róg, M. Karttunen and I. Vattulainen, *J. Phys. Chem. B*, 2008, **112**, 2922–2929.
59 J. Aittoniemi, T. Róg, P. Niemelä, M. Pasenkiewicz-Gierula, M. Karttunen and I. Vattulainen, *J. Phys. Chem. B*, 2006, **110**, 25562–25564.
60 G. Khelashvili, G. Pabst and D. Harries, *J. Phys. Chem. B*, 2010, **114**, 7524–7534.
61 M. Alwarawrah, J. Dai and J. Huang, *J. Phys. Chem. B*, 2010, **114**, 7516–7523.
62 H. M. McConnell and A. Radhakrishnan, *Biochim. Biophys. Acta*, 2003, **1610**, 159–173.
63 P. L. Chong, *Proc. Natl. Acad. Sci. U. S. A.*, 1994, **91**, 10069–10073.
64 M. R. Ali, K. H. Cheng and J. Huang, *Proc. Natl. Acad. Sci. U. S. A.*, 2007, **104**, 5372–5377.
65 X. Lin, Y. Li and N. Gu, *J. Comput. Theor. Nanosci.*, 2010, **7**, 269–276.
66 S. J. Marrink and H. J. C. Berendsen, *J. Phys. Chem.*, 1994, **98**, 4155–4168.
67 S. J. Marrink and H. J. C. Berendsen, *J. Phys. Chem.*, 1996, **100**, 16729–16738.
68 D. Bemporad, J. W. Essex and C. Luttmann, *J. Phys. Chem. B*, 2004, **108**, 4875–4884.
69 E. Falck, M. Patra, M. Karttunen, M. T. Hyvönen and I. Vattulainen, *J. Chem. Phys.*, 2004, **121**, 12676.

